HHS Public Access

Author manuscript

Biomed Pharmacother. Author manuscript; available in PMC 2022 August 24.

Published in final edited form as:

Biomed Pharmacother. 2022 June ; 150: 112928. doi:10.1016/j.biopha.2022.112928.

Small molecules targeting the NADH-binding pocket of VDAC modulate mitochondrial metabolism in hepatocarcinoma cells

Kareem A. Heslop[a], **Pieter Burger**[a], **Christiana Kappler**[b], **Ashish K. Solanki**[d], **Monika Gooz**[a], **Yuri K. Peterson**[a], **Catherine Mills**[a], **Thomas Benton**[a], **Stephen A. Duncan**[b], **Patrick M. Woster**[a], **Eduardo N. Maldonado**[a,c,*]

[a]Department of Drug Discovery & Biomedical Sciences, Medical University of South Carolina, Charleston, SC, USA

[b]Regenerative Medicine and Cell Biology, Medical University of South Carolina, Charleston, SC, USA

[c]Hollings Cancer Center, Medical University of South Carolina, Charleston, SC, USA

[d]Nephrology Division, Medical University of South Carolina, Charleston, SC, USA

Abstract

Voltage dependent anion channels (VDAC) control the flux of most anionic respiratory substrates, ATP, ADP, and small cations, crossing the outer mitochondrial membrane. VDAC closure contributes to the partial suppression of mitochondrial metabolism that favors the Warburg phenotype of cancer cells. Recently, it has been shown that NADH binds to a specific pocket in the inner surface of VDAC1, also conserved in VDAC2 and 3, closing the channel. We hypothesized that binding of small molecules to the NADH pocket, maintain VDAC in an open configuration by preventing closure induced by NADH and possible other endogenous regulators. We screened *in silico,* the South Carolina Compound Collection SC^3 (~ 100,000 proprietary molecules), using shape-based queries of the NADH binding region of VDAC. After molecular docking of selected compounds, we physically screened candidates using mitochondrial membrane potential ($\Delta\Psi m$), as an overall readout of mitochondrial metabolism. We identified **SC18,** as the most potent compound. **SC18** bound to VDAC1, as assessed by a thermal shift assay. Short-term treatment with **SC18** decreased $\Delta\Psi m$ in SNU-449 and HepG2 human hepatocarcinoma cells. Mitochondrial depolarization was similar in wild type, VDAC1/2, 1/3, and 2/3 double KO HepG2 cells indicating that the effect of **SC18** was not VDAC isoform-dependent. In addition, **SC18** decreased mitochondrial NADH and cellular ATP production; and increased basal respiration.

*Correspondence to: Department of Drug Discovery & Biomedical Sciences, Medical University of South Carolina, DD506 Drug Discovery Building, 70 President Street, MSC 139, Charleston, SC 29425, USA. maldona@musc.edu (E.N. Maldonado).

CRediT authorship contribution statement

KA Heslop: experimentation, data processing, writing. **P Burger**: in silico screening, molecular modeling. **C. Kappler** and **SA Duncan**: CRISPR-Cas9 developments. **AK Solanki**: recombinant technology. **Gooz, M:** imaging methodologies. **YK Peterson:** drug discovery. **C Mills** and **T Benton:** compound synthesis. **PM Woster:** drug discovery supervision. **EN Maldonado:** team organization and supervision, experimental designs, data interpretation, writing and final editing.

Conflict of interest statement

The authors declare that they have no known competing financial interests or personal relationships that could have appeared to influence the work reported in this paper.

Long-term exposure to **SC18**, decreased cell proliferation as determined by wound-healing and cell viability assays. In summary, **SC18** is a novel VDAC-targeting small molecule that induces mitochondrial dysfunction and inhibits cell proliferation.

Keywords

VDAC; Mitochondrial metabolism; Cancer; NADH-binding pocket; Mitochondrial dysfunction

1. Introduction

Cancer bioenergetics and cancer metabolism are contributed both by aerobic glycolysis and oxidative phosphorylation (Oxphos). In the early 20th century, Warburg showed that at physiological partial pressures of oxygen, tumors produce more lactic acid than non-tumor tissues [1,2]. Warburg even proposed that damaged mitochondria were the origin of cancer, a theory proved wrong shortly after. In fact, both high glycolysis and oxidative metabolism contribute to tumor cell metabolism in different proportions [3-9]. The current consensus is that the Warburg phenotype favors proliferation by providing carbon backbones and metabolic intermediaries needed for the synthesis of biomass [10-12]. The relative contribution of mitochondria to generation of ATP and metabolic intermediaries, varies among tumor types, within the same tumor, and during tumor growth, indicating a spatiotemporal dynamic regulation of oxidative metabolism. The interdependency between enhanced glycolysis and mitochondrial metabolism, is a key feature contributing to the metabolic heterogeneity, increasingly recognized as a cause of failure in chemotherapy. Thus, mitochondria appear as an attractive target to develop novel “metabolic” treatments to inhibit cell proliferation [13-17].

Maintenance of mitochondrial metabolism depends on the balance between the influx of respiratory substrates, cytosolic ATP, ADP, inorganic phosphate and small ions into mitochondria; and the efflux of ATP and metabolic intermediaries to the cytosol. To reach the mitochondrial matrix, most anionic metabolites and small ions cross the outer mitochondrial membrane (OMM) through Voltage dependent anion channels (VDAC). VDAC (~30 kDa), is the most abundant protein in the outer mitochondrial membrane, comprising three isoforms. In most mammalian cells, VDAC1 and 2 are the most abundant, whereas VDAC3 is the least expressed isoform, except for testis and spermatozoa [18,19]. NMR and X-ray crystallography have shown that VDAC1 and 2, form a transmembrane β-barrel protein, with 19 anti-parallel β-strands and an N-terminal α-helical region located within the pore [20,21]. VDAC inserted in non-polarized or weakly polarized membranes (close to 0 mV), stays mostly in the high conductance open state. By contrast, applied positive or negative membrane potentials induce conformational changes to several lower conductance, closed states (maximal at - or +45 mV) [22,23]. Although gating and selectivity for VDAC1 and VDAC2 are very similar in different cell types, the molecular mechanisms of VDAC voltage gating are still incompletely understood.

Regardless of the mechanism controlling gating, the flux of polar metabolites through VDAC is determined mostly by their charge and size [24,25]. VDAC is selective for anionic

metabolites and small cations [26-28]. The open state of VDAC allows the flux of anions including most respiratory substrates, ATP^{4-}, ADP^{3-}, AMP, HPO_4^{2-}, and phosphocreatine, among others. In the closed states, VDAC favors a non-selective flux of cations including Na^+, K^+, and Ca^{2+} [29-31]. Consequently, physiological or pharmacological regulations that induce a change from the open state to the closed states of VDAC, decrease and increase the flux of negatively charged metabolic substrates and cations, respectively. Even though VDAC was initially considered an "all-time open gateway", allowing the unrestricted flux of metabolites, subsequent research showed multiple endogenous regulations. NADH, α/β tubulin heterodimers, hexokinase-II, alpha-synuclein, p53, bcl2 family members and mitochondrial creatine kinase regulate VDAC opening [32-34]. Post-translational modifications, mainly phosphorylation by protein kinases, GSK3β, PKA, and protein kinase C epsilon (PKCε), inhibit association of VDAC with other proteins and also regulates VDAC opening [35-37].

Overall, the movement of metabolites through VDAC depends on the concentration gradient across the OMM, the electric field, the number of channels, the selectivity-permeability to a particular metabolite, and the open probability of the channel. Thus, VDAC emerges as a potential pharmacological target to modulate mitochondrial metabolism in cancer cells. However, major limitations to develop VDAC-targeting drugs have been the isoform specificity, the lack of an identified druggable region, and a poor understanding of mechanisms regulating gating of the channel. Moreover, the mechanisms of action of several compounds, claimed to bind to VDAC, remain unknown. Recently, an NADH-binding pocket in VDAC1, with an amino acid sequence conserved in all VDAC isoforms, has been identified [38]. Binding of β-NADH to the pocket reduces VDAC conductance by steric occlusion of the pore without changes at the α-helix, suggesting that molecules binding to this site may prevent VDAC closing by endogenous regulators.

Here, we hypothesize that small molecules targeting the NADH-binding pocket of VDAC will block the binding of NADH and possibly other endogenous regulators to the site, maintaining the channel in an open configuration. Using an *in silico* approach followed by biological assays, we identified the lead compound **SC18**. Short-term treatment with **SC18**, decreased mitochondrial membrane potential ($\Delta\Psi m$), NADH and ATP, and increased basal respiration. Long-term exposure to **SC18** decreased cell proliferation and promoted cell death in a dose-dependent fashion. Our results suggest that decreased cell proliferation and cell death induced by **SC18** was caused by mitochondrial dysfunction.

2. Methods

2.1. Materials

Antimycin A, carbonyl cyanide 3-chlorophenylhydrazone (CCCP), oligomycin, rotenone, zosuquidar, and tetramethylrhodamine methyl ester (TMRM), were purchased from Millipore Sigma (Burlington, MA). Fetal bovine serum (FBS) was from Atlanta Biologicals. Penicillin, streptomycin, 100X MEM nonessential amino acids, and RPMI 1640 containing 2.05 mML-glutamine, were from Thermo Fisher Scientific (Waltham, MA, USA). Eagle's

Minimum Essential Medium was from the American Type Culture Collection (ATCC; Manassas, VA, USA). All other chemicals were analytical grade.

2.2. Virtual screening

We used a virtual screening strategy to identify novel compounds targeting the NADH-binding pocket. We chose an NMR structure of VDAC (PDB: 6TIR), solved with NADH bound within the pore among the 12 X-ray or NMR structures resolved for VDAC [38]. NADH binding reduces the conductance of the pore sterically without triggering a structural change. We used the NADH pocket for the virtual screening of the South Carolina Compound Collection SC3 comprised of over 130,000 compounds, including 100,000 proprietary and fully annotated drug-like molecules. To optimize the screen, we used the nicotinamide moiety and adjacent phosphate groups that is resolved in a well-defined pocket to generate shape-based queries, while omitting the adenosine moiety that freely rotates within the channel. The shape-based virtual screening, using the OpenEye software ROCS (OpenEye Scientific Software, Inc), assumes that compounds with similar shape and electrostatic characteristics will bind to the same target. We next performed molecular docking of the top 20,000 compounds using the extra precision (XP) scoring function against VDAC1 (Glide; Schrodinger Inc). The top 500 scoring compounds, identified based on the lowest scoring docking energy, were visually inspected to select 72 compounds for physical screening using $\Delta\Psi m$ as a readout of mitochondrial metabolism.

2.3. Expression and purification of recombinant human VDAC1

pET-29a recombinant human VDAC1 (rhuVDAC1) Open Reading Frame (ORF) clone plasmid construct, was purchased from GenScript and confirmed using sequencing. The plasmid was transformed into expression strain BL21 (DE3) (ThermoFisher) bacteria grown in Luria-Bertani media containing 50 μg/mL kanamycin. The expression of the His-tagged rhuVDAC1 was induced by 1 mM isopropyl-β-D-thiogalactopyranoside (IPTG) for 4 h at 37 °C with vigorous shaking. Bacteria were then harvested by centrifugation at 6000 rpm at 4° C for 10 min. The biomass (6–7 g/L) obtained was resuspended in buffer A (1:50 v/v, 20 mM Tris, pH 7.9, 200 mM NaCl, 1 mM phenylmethylsulfonyl fluoride (PMSF), EDTA free 1X protease inhibitor cocktail). Resuspended bacteria were incubated with 0.5 mg/mL of lysozyme on ice for 30 min and lysed by pulse sonication. Inclusion bodies were washed in buffer A before solubilizing in buffer B (1:20 v/v, 4 M guanidine–HCl, 20 mM Tris–HCl, pH 7.9, 500 mM NaCl, and 10% glycerol) at 4° C for 30 min with gentle stirring. The supernatant containing the denatured rhuVDAC1 was collected by centrifugation at 15,000 g for 30 min. Buffer B (containing~ 20 mg total soluble proteins) was incubated with 1 mL of Nickel-Nitriloacetic acid (Ni-NTA) Superflow Agarose beads; before incubation with 5 mL of denatured protein supernatant for 2 h, followed by washing with buffer B. Further 3-step wash with buffer B mixed with buffer C (2% n-octyl-b-D-glucopyranoside (OG), 20 mM Tris, pH 7.9, 500 mM NaCl, and 10% glycerol) plus 10 mM imidazole (B:C = 1:3, 1:7, and 1:15, respectively) was performed to ensure maximal refolding and renaturing of the protein, and to remove excessive impurity. Additional washes with buffer C and 10 mM imidazole removed excess of guanidine, before the His-tagged rhuVDAC1 was eluted by gravity using buffer C supplemented with 300 mM imidazole at 4 °C. Protein fractions were dialyzed

against buffer C for 4–6 h. Final purity and identity of the target proteins were confirmed by analyzing the bands in SDS-PAGE and western blot.

2.4. Cell culture

HepG2 (Cat # HB-8065) and SNU-449 (Cat # CRL-2234) human hepatocellular carcinoma, were purchased from the American Tissue Culture Collection (ATCC) (Manassas, VA). HepG2 cells were grown in Eagle's minimum essential medium (EMEM) supplemented with 10% fetal bovine serum (FBS) premium (Atlanta Biologicals), 100 units/mL penicillin and 100 μg/mL streptomycin. SNU-449 cells were grown in RPMI-1640 with the addition of 10% fetal bovine serum (FBS) premium (Atlanta Biologicals), 100 units/mL penicillin and 100 μg/ mL streptomycin. Both cell lines were maintained in 5% CO_2/air at 37 °C. All experiments were performed when cells reached 70–80% confluency.

2.5. VDAC KO cells

sgRNA sequences targeting Exon 4 of VDAC 1, Exon 5 of VDAC2 and Exon 5 of VDAC3 were designed using Synthego (Synthego, Redwood City, CA) or CRISPOR (http://crispor.tefor.net/) and synthesized by IDT (IDT, San Diego, CA). sgRNA sense and antisense strands were: VDAC1, ACTAGGCACCGAGATTACTG and CAGTAATCTCGGTGCCTAGT; VDAC2, CGCGCGTCGTAAGTAAAGCT and AGCTTTACTTACGACGCGCG; VDAC3, GACCAGAAGTAGAAAATTCC and GGAATTTTCTACTTCTGGTC.

Each of the guide RNA sequences were cloned into the PX459 pSPCas9 (BB)-2A-Puro vector. For transfection, HepG2 cells were plated at approximately 50% confluence in 10 cm tissue culture dishes. The following day, cells were transfected with 30 μg of total sgRNA, 15 μg each, in the following combinations: VDAC1/VDAC2, VDAC1/ VDAC3, and VDAC2/ VDAC3 using Viafect (Promega, Cat. # E4981), according to the manufacturer's protocol. After 24 h, the media was changed to EMEM, 10% FBS + puromycin 1 ug/ul for 48–72 h, until all cells in a negative-control plate treated with selection media were dead. Following selection, cells were maintained in EMEM 10% FBS and allowed to grow until colonies were visible. Colonies were then transferred into each well of a 96-well plate and allowed to grow for an additional 2–3 d. Colonies were dissociated with trypsin and divided between two 96 well plates. After 2–3 d of growth, the wells of one plate were harvested using 50 μL QuickExtract (QuickExtract, Middleton, WI), following the manufacturer's instructions. Extracted DNA was used for PCR with primers designed to amplify the target region. Forward and reverse primers were: VDAC1, GTGCAGGCTGTGACTCTTCT and AAGGTCAGCTTCAGTCCACG; VDAC2, AGGGAGGAAGGAAGCTGTCTGC and GTCACAAAGGGCTTCCACCACC; VDAC3, GCTGGTCTTGAGCTCCTGGACT and ACCCAGGAGAAGCTTAGCTGTGT.

Following PCR amplification, the products were digested with enzymes with recognition sites near the sgRNA cut site (VDAC1 – *Mbo*I, VDAC2 – *Alu*I, and VDAC3 – *Apo*I). If CRISPR-Cas9 modification was successful, the enzyme would fail to digest the PCR product. When potential hits were identified, PCR products of the target regions were sequenced and ICE analysis (Synthego), was used to identify and confirm knockout success.

2.6. Confocal microscopy of TMRM and NADH

HepG2 and SNU-449 cells were plated in Grenier Bio-One TC 4-chamber plates (Greiner-Bio-One, Monroe, NC), or 35 mm MatTek dishes (MatTek Corporation, Ashland, MA). Cells were loaded with 20 nM TMRM for 60 min in modified Hank′s balanced salt solution (HBSS) containing (in mM): NaCl 137, Na_2HPO_4 0.35, KCl 5.4, KH_2PO_4 1, MgSO4 0.81, Ca_2Cl 0.95, glucose 5.5, $NaHCO_3$ 25 and HEPES 20, pH 7.4. Live cells, maintained in the Zeiss LSM 880 NLO inverted laser scanning confocal microscope (Thornwood, NY) environmental chamber (humidified 5% CO_2 at 37 °C), were imaged with a 63 × 1.4 N.A. plan apochromat oil immersion lens. TMRM was excited at 561 nm. Emission was detected with a Quasar multichannel spectral detector at 590–610 nm through a one Airy unit diameter pinhole. TMRM intensities were quantified to make relative comparisons using Photoshop CS4 software (Adobe Systems, San Jose, CA) as previously described [32,39]. A minimum of 4 randomly selected fields with 8–20 cells per field were imaged during the time course of 3 independent experiments for all microscopy experiments.

NADH autofluorescence was imaged using multiphoton laser excitation (720 nm, 3% power) and an emission barrier filter (460 ± 25 nm). TMRM and NADH intensity were quantified using Zeiss Zen and Photoshop CS4 (Adobe Systems, San Jose, CA, USA) software after subtraction of background fluorescence as previously described [40,41].

2.7. ATP measurement

ATP was determined in cells lysed with the luciferase-based Cell Titer-Glo Luminescent Assay Kit (Promega, WI, Cat # G7570). Luminescence was measured in a Biotek Synergy H1 plate reader. All luminescence values were normalized per million cells, and expressed as percentage compared to vehicle.

2.8. Respirometric assay

Oxygen consumption rates (OCR) were measured using a Seahorse XF96 analyzer (Agilent Technologies, Santa Clara, CA, USA), and calculated from the continuous average slope of the O_2 partitioning among plastic, atmosphere, and cellular uptake [42,43]. SNU-449 or HepG2 cells (25,000/ well) in XF96-well microplates were maintained in growth media and treated 24 h after plating. Experiments were performed in 200 μL/ well of respiratory substrate (RS) buffer containing (in mM): L-glutamine 4, D-Glucose 10, sodium pyruvate 1, $CaCl_2$ 0.036, $MgCl_2$ 0.06, KH_2PO_4 0.05, KCl 0.54, Na_2HPO_4 heptahydrate 0.05, HEPES 2 and NaCl 13 (pH: 7.4). Microplates and sensor cartridges were kept in an air incubator for 1 h before starting the experiments. Basal, oligomycin sensitive, and maximal respiratory capacity were determined after sequential addition of oligomycin (1 μM), CCCP (1 μM), and rotenone (2 μM) + antimycin A (2 μM), respectively.

2.9. Wound healing

SNU-449 cells were plated in 2-wells Ibidi culture-inserts (Gräfelfing, Germany). After overnight incubation, inserts were removed and cells were washed with PBS. Fresh medium containing **SC18**, sorafenib, or vehicle was then added to the culture plate, which was incubated using a humidified 5% CO_2/ air at 37 °C in a BIOTEK Cytation 5 multimode

(imaging) reader equipped with a BioSpa automated incubator and MultiFlo liquid handler (Agilent, CA, USA). The entire plate was imaged in a time-lapse mode every 4 h for 2 d.

2.10. EC50

SNU-449 cells plated in glass bottom, 10-well Cellview culture slides (Greiner-Bio-One), were incubated with 20 nM TMRM in HBSS for 1 h. EC50 was calculated assessing mean intensity of TMRM fluorescence (GraphPad Prism, San Diego, CA) after 2 h exposure to **SC18** at increasing concentrations.

2.11. LC50

SNU-449 cells plated in 6-well tissue culture plates (VWR, Radnor, NC) were exposed to **SC18** at increasing concentrations for 5 d. Cell viability was determined using a trypan blue exclusion assay and calculated using GraphPad Prism.

2.12. Statistical analysis

Statistical differences between groups were analyzed by the Student's t-test using $p < 0.05$ as the criterion of significance. Data points are the means ± S.E. of 3–5 independent experiments. Images in figures are representative of three or more independent experiments unless otherwise described.

3. Results

3.1. Identification of SC18

To identify small molecules targeting the NADH-binding pocket of VDAC, we screened *in silico* the South Carolina Compound Collection SC[3]. We chose an NMR structure of VDAC, solved with NADH bound within the pore. To specifically target the NADH-binding pocket, we only used the nicotinamide moiety, that interacts directly with the pocket, and the sugar ring attached to a phosphate molecule, while omitting the adenine group that sterically occludes the lumen of VDAC1. The shape-based virtual screening, that assumes that compounds with similar shape and electrostatic characteristics will bind to the same target, was followed by molecular docking of the top 20,000 compounds. The top 500 scoring compounds, identified based on the lowest scoring docking energy, were visually inspected to select 72 compounds for physical screening (Fig. 1). Since VDAC opening modulates mitochondrial metabolism, we chose assessment of $\Delta\Psi m$ by confocal microscopy of TMRM fluorescence, as a method to globally assess mitochondrial function in intact cells. Although $\Delta\Psi m$ is modulated by several factors, changes induced by short-term pharmacological treatments are robust indicators of drug-induced changes in mitochondrial metabolism. To discard compounds with a mild effect on mitochondrial function, we established an arbitrary threshold of 40% change in TMRM fluorescence compared to baseline, as a criterion to select hits. This strategy led to the identification of **SC18** as our most potent hit (Figs. 1 and 2A).

3.2. Assessment of SC18 binding to VDAC

The potential binding of **SC18** to the target was assessed using both an *in silico* and a wet-lab approach. To determine the stereochemistry of **SC18** in the NADH binding pocket of VDAC1 (NMR structure, 6TIR), we overlaid the docking poses of **SC18** and β-NADH. The predicted binding poses of **SC18** indicated a very similar orientation compared to β-NADH bound to the pocket. A schematic diagram of *in silico* docking of NADH bound to the NMR structure of VDAC superimposed with **SC18** is shown in Fig. 2B. The quinazolinedione scaffold forms two hydrogen bonds with lysine 20, one with the backbone and the terminal nitrogen; and other similar interactions to the ring oxygen from the sugar ring closest to the 1, 4 dihydronicotinamide moiety of NADH. Two pi-cation interactions were found between the quinazoline-dione and Arginine 218. The 6-nitro substitution formed a hydrogen bond with Tyrosine 22, similar to the phosphate backbone of NADH. In addition, the trifluoromethyl overlays with an amide moiety of the 1,4-dihydronicotinamide of NADH in the binding pocket. To determine actual binding to VDAC1, we incubated **SC18** with recombinant VDAC1 purified from E. Coli [44]. We performed an isothermal calorimetric assay with β-NADH as positive control, using a NanoTemper Tycho NT. 6. Addition of **SC18** to VDAC1, similar to β-NADH, caused a temperature shift of ~7 °C indicating that **SC18** binds to VDAC1 (Fig. 2C). The combined *in silico* and wet-lab approach strongly suggests that **SC18** binds to the VDAC NADH-binding pocket.

3.3. SC18 modulates mitochondrial metabolism

3.3.1. Mitochondrial membrane potential—To initially assess the effects of **SC18** on mitochondrial metabolism and determine the EC50, we quantitatively assessed ΔΨm. Maintenance of ΔΨm depends on an adequate influx of ADP, inorganic phosphate, and respiratory substrates to fuel the Krebs cycle, and a functional electron transport chain coupled to ATP synthesis. Thus, quantitative measurement of ΔΨm is an overall indicator of mitochondrial metabolism. We loaded HepG2 and SNU-449 cells with the fluorophore potential indicator TMRM, a cation that accumulates in proportion to the negative charges in the mitochondrial matrix. Changes in a non-quenching mode of TMRM fluorescence reflect changes in ΔΨm in a linear fashion. Treatment with **SC18** for 2 h, decreased ΔΨm by ~ 50% compared to vehicle in wild type (wt) HepG2 and SNU-449 cells (Fig. 3 and not shown). To determine if the drop in ΔΨm caused by **SC18** depended on the presence of a specific VDAC isoform, we used **SC18** at the same concentration in wt and in VDAC1/2, VDAC1/3 and VDAC2/3 double KO HepG2 cells. **SC18** (25 μM) decreased ΔΨm similarly in Wt, VDAC 1/2, 2/3, and 1/3 double KO cells (~ 52%, 46%, 61%, and 44% respectively) indicating that the depolarizing effect of **SC18** was not isoform dependent (Fig. 3A and B.). The results also suggest that **SC18** very likely targets all VDAC isoforms. We also used changes in ΔΨm after treatment with **SC18** as a readout to determine EC50, that was established at 25 μM (Fig. 3C).

3.3.2. NADH generation—Oxidation of pyruvate, fatty acids and certain amino acids in the Krebs cycle generates NADH that is the main donor of electrons to the respiratory chain. NADH levels are modulated by the influx of substrates to support the Krebs cycle in the mitochondrial matrix, and the utilization of NADH by the respiratory chain to support the

synthesis of mitochondrial ATP. To assess whether **SC18** influenced mitochondrial NADH generation, we assessed NADH autofluorescence by multiphoton fluorescence microscopy. **SC18** for 2 h decreased mitochondrial NADH by~ 15% in HepG2 cells (Fig. 4 A-B). This finding may suggest an increased utilization of NADH or a decreased activity of the Krebs cycle induced by **SC18**.

3.3.3. Respiration and ATP production—Since changes in ΔΨm and mitochondrial NADH are not necessarily correlated with changes in oxidative phosphorylation, we determined if **SC18** induced changes in respiration (assessed as oxygen consumption rates) and ATP production using a luminescence assay.

SC18 at 1, 3, 10, or 30 μM for 2 h increased basal respiration in a dose-dependent fashion after treatment from 154 pmol/ min/ 3.5 $\times 10^4$ cells to a maximum of~ 243 pmol/ min/ 3.5 $\times 10^4$ cells at 30 μM (Fig. 4C). **SC18** (30 μM) for 2 h, also decreased cellular ATP by~ 24% (Fig. 4D). Taking together, these results suggest that the increase in oxygen consumption, was not triggering a proportional increase in ATP synthesis, as it would be expected in fully coupled mitochondria.

3.4. SC18 is cytotoxic

3.4.1. Cell viability—The effects of **SC18** on mitochondrial metabolism, assessed in the first 2 h after treatment with the small molecule, did not affect cell viability. To determine if sustained metabolic changes would lead to inhibition of cell proliferation and cell death after long-term exposure to **SC18**, we assessed cell viability using a trypan blue exclusion assay. Using this method, we determined an LC50 of 24 μM after 5 d treatment (Fig. 5A).

3.4.2. Wound healing—After confirming the short-time effects on mitochondrial metabolism and the long-term effects on cell viability, we studied if **SC18** would also inhibit cell migration and proliferation. For that purpose, we used a scratch assay, and imaged cells every 8 h up to 48 h after treatment with **SC18** (24 μM) (Fig. 5B). As a positive control, we used sorafenib (5 μM), a chemotherapeutic agent that promote death in hepatocarcinoma cells. Both **SC18** and sorafenib delayed wound healing similarly. The maximal inhibitory effect (50% inhibition), occurred 24 h after treatment. 48 h after treatment, the inhibitory effect of **SC18** on wound healing was stil ≃30%. This result indicates that the early effects of **SC18**, likely sustained over time, leads to inhibition of both cell proliferation and cell death.

4. Discussion

In almost all proliferating and non-proliferating eukaryotic cells, VDAC1 and 2 are the most abundant isoforms, except for testis and spermatozoa in which VDAC3 is more abundant. Regardless of the extensive research on VDAC structure and function in reconstituted systems, many questions about VDAC regulation and function in physiological and pathological conditions remain undetermined. A potential redundancy in function and different metabolic roles for each isoform, proposed as likely happening in the intracellular milieu, have not been supported by experimental data. Research efforts have been also dedicated to disrupt the interaction between VDAC and hexokinase-II as a mechanism to

target mitochondrial function for cancer therapy. Recently, it has been shown that a series of cell permeant amphiphilic peptides that disrupt the interaction between VDAC1 and HK-II induce apoptosis in melanoma and lung carcinoma cells [45-47]. From a pharmacological perspective, the success of modulating VDAC opening is most likely to occur if the three isoforms are targeted simultaneously. However, VDAC isoform specificity and lack of identifiable druggable sites, have been big obstacles for the development of drugs regulating VDAC [32,48].

In previous work from our group, we showed that VDAC1, 2 and 3 are major contributors to mitochondrial metabolism in cancer cells. Single or double kd of VDAC isoforms in all combinations, decreased ΔΨ. In particular, kd of the minor isoform VDAC3 in HepG2 cells caused the maximum decrease in ΔΨm, ATP and NADH. We also demonstrated that free tubulin dynamically modulates ΔΨm and inhibits VDAC1 and VDAC2 in cancer cells [4,32]. Additional work from our group identified erastin and a series of erastin-like molecules as antagonists of the VDAC-tubulin interaction [49]. VDAC opening induced by VDAC-tubulin antagonists led to increased oxidative metabolism, accumulation of ROS, mitochondrial dysfunction, reversal of the Warburg metabolism and cell death [49,50].

Recently, it has been shown that binding of NADH to a specific pocket in VDAC1 induces closure of the channel [38]. We analyzed the sequence of residues in the VDAC1 NADH-binding pocket and found that it is fully conserved in VDAC2 and 3. Thus, we hypothesized that the NADH-binding pocket was an excellent pharmacological target to identify small molecules to occupy the site, prevent the binding of endogenous regulators, and maintain all VDAC isoforms open. Because of the stereochemical characteristics of the pocket, we used the nicotinamide moiety and adjacent phosphate groups to generate shape-based queries to screen *in silico* the South Carolina Compound Collection SC^3. After subsequent modeling including molecular docking of initial candidates, we identified **SC18** as a hit compound. We also proved that **SC18** binds to VDAC1. The thermal shift assay that we used indicates if the compound binds or not to the protein, but has the limitation of not identifying specifically an intramolecular binding site. A precise determination of **SC18** binding to the NADH-binding pocket would require soaking VDAC1 crystals in the presence of the compound followed by NMR to identify the binding. Although it is a very interesting prospective, because of the methodological difficulties involved, this approach is out of the scope of the current work.

Our *in silico* strategy was followed by biological assays to identify the most potent hit. Initially, we used ΔΨm as the readout because it is a global indicator of mitochondrial function. Maintenance of ΔΨm depends on an adequate flux of metabolites through VDAC, but also on the activity of the Krebs cycle and coupled oxidative phosphorylation. However, ΔΨm is subjected to multiple levels of regulation and increases or decreases in ΔΨ do not necessarily imply a change in VDAC opening or closing states. Because of this caveat and to use a multidimensional approach, we studied other indicators of mitochondrial function. After identifying **SC18** as the most potent compound decreasing ΔΨm, we studied mitochondrial NADH generation, ATP production and respiration. Most mitochondrial NADH is produced by the oxidation of respiratory substrates in the Krebs cycle. NADH, in turn, is the main electron donor for the respiratory chain. Electrons

originated from NADH enters the chain at complex I, and flow through complexes II, III, and IV to the final acceptor oxygen. The activity of the ETC generates protons pumped to the intermembrane space. Those protons are the main component of the proton motive force that maintains ΔΨ and is used to generate ATP by the ATP synthase. Similar to ΔΨm, NADH and ATP generation decreased in the presence of **SC18**. Although decreased ΔΨm, NADH and ATP would be consistent with decreased mitochondrial metabolism, the increase in respiration induced by the lead compound, seems to contradict this interpretation. It is possible that **SC18** exerts a time dependent biphasic effect. If, according to our hypothesis **SC18** block the access of endogenous regulators to the NADH-binding pocket, it would be reasonable to expect a transient increase in mitochondrial metabolism followed by mitochondrial dysfunction. Thus, decreased ΔΨm, ATP, and NADH would reflect mitochondrial dysfunction. Two likely scenarios to explain the increase in respiration caused by **SC18** are related to a potential activation of parallel proton re-entry pathways competing for protons with the ATP synthase. In general, proton conductance attributable to the phospholipid bilayer of the mitochondrial inner membrane is only 5%. The re-entry of protons in intact mitochondria occur mostly through uncoupling proteins and possibly the adenine nucleotide translocator [51,52]. More recently, the subunit c of the ATP synthase has been shown to control proton leak in neurons [53,54]. Although the subunit c is a major controller of the leak in neurons, it remains unknown if a similar mechanism could also control proton leak in cancer cells. In any case, more time-course studies will be necessary to determine if the effects of **SC18** on respiration are specific to VDAC opening or involve other non-specific targets as those mentioned above.

Mitochondria, that contribute 10–90% of total cellular ATP in cancer cells, is also an essential source of metabolic intermediaries for the synthesis of biomass. Thus, changes in mitochondrial metabolism may impact very differently not only cellular metabolism but also cell proliferation. In that sense, we evaluated if the decrease in mitochondrial function was followed by a decrease in cell proliferation. We showed that long-term treatment with **SC18** (3–5 d), delays wound healing. Since wound healing assays assess not only proliferation but migration as well, we confirmed the inhibitory effect of **SC18** on cell proliferation by quantifying cell viability and proliferation using Trypan blue exclusion and direct counting. Our results clearly indicated an inhibitory effect of **SC18** on cell proliferation starting at 10 μM. However, cell death (≃ 96%) was only observed at maximal concentrations (30 μM).

Future experimentation will be required to determine if **SC18** regulates the conductance of VDAC inserted into lipid bilayers and the mechanisms triggering the increase in respiration after treatment with the small molecule. In addition, the drug discovery process will continue to generate more potent and specific analogues of **SC18**.

In summary, our findings show that **SC18** modulates mitochondrial metabolism in cancer cells, inhibit cell proliferation and induce cell death. Thus, **SC18,** may become the first of a series of specific VDAC-targeted modulators of mitochondrial metabolism.

Acknowledgements

This work was supported, in part, by the U.S. National Institutes of Health (NIH/NCI) RO1 CA184456, and South Carolina Translational Research Pilot Project UL1 TR001450-SCTR to E.N.M; the Chan Zuckerberg Foundation

Imaging Scientist Award to M.G., and the Abney Foundation Fellowship from MUSC Hollings Cancer Center, to K.H. Authors declare no conflicts of interest. MUSC COBRE in Digestive and Liver Disease Cell Models Core generated the CRISPR-Cas9 knockout cells used in this study. The *in silico, synthetic chemistry and medicinal chemistry procedures described in this manuscript were conducted by the MUSC Drug Discovery Core*.

Abbreviations:

ΔΨm	mitochondrial membrane potential
Oxphos	oxidative phosphorylation
SOR	sorafenib

References

[1]. Warburg O, Ueber den Stoffwechsel der Tumoren, Constable, London, 1930, p. 1930.

[2]. Warburg O, Wind F, Negelein E, The metabolism of tumors in the body, J. Gen. Physiol 8 (6) (1927) 519–530. [PubMed: 19872213]

[3]. Lim HY, Ho QS, Low J, Choolani M, Wong KP, Respiratory competent mitochondria in human ovarian and peritoneal cancer, Mitochondrion 11 (3) (2011) 437–443, doi: S1567-7249(10)00235-7 [pii];10.1016/j.mito.2010.12.015 [doi]. [PubMed: 21211574]

[4]. Maldonado EN, Patnaik J, Mullins MR, Lemasters JJ, Free tubulin modulates mitochondrial membrane potential in cancer cells, Cancer Res. 70 (24) (2010) 10192–10201, 10.1158/0008-5472.CAN-10-2429. [PubMed: 21159641]

[5]. Mathupala SP, Ko YH, Pedersen PL, The pivotal roles of mitochondria in cancer: Warburg and beyond and encouraging prospects for effective therapies, Biochim Biophys. Acta 1797 (6–7) (2010) 1225–1230, doi: S0005-2728(10)00131-3 [pii];10.1016/j.bbabio.2010.03.025 [doi]. [PubMed: 20381449]

[6]. Moreno-Sanchez R, Marin-Hernandez A, Saavedra E, Pardo JP, Ralph SJ, Rodriguez-Enriquez S, Who controls the ATP supply in cancer cells? Biochemistry lessons to understand cancer energy metabolism, Int. J. Biochem. Cell Biol 50 (2014) 10–23, doi: S1357-2725(14)00042-9 [pii];10.1016/j.biocel.2014.01.025 [doi]. [PubMed: 24513530]

[7]. Nakashima RA, Paggi MG, Pedersen PL, Contributions of glycolysis and oxidative phosphorylation to adenosine 5′-triphosphate production in AS-30D hepatoma cells, Cancer Res. 44 (12 Pt 1) (1984) 5702–5706. [PubMed: 6498833]

[8]. Singleterry J, Sreedhar A, Zhao Y, Components of cancer metabolism and therapeutic interventions, Mitochondrion 17C (2014) 50–55. S1567-7249(14) 00084-1 [pii];10.1016/j.mito.2014.05.010 [doi].

[9]. Guppy M, Leedman P, Zu X, Russell V, Contribution by different fuels and metabolic pathways to the total ATP turnover of proliferating MCF-7 breast cancer cells, Biochem. J 364 (Pt 1) (2002) 309–315. [PubMed: 11988105]

[10]. DeBerardinis RJ, Sayed N, Ditsworth D, Thompson CB, Brick by brick: metabolism and tumor cell growth, Curr. Opin. Genet. Dev 18 (1) (2008) 54–61, 10.1016/j.gde.2008.02.003. [PubMed: 18387799]

[11]. Vander Heiden MG, Cantley LC, Thompson CB, Understanding the Warburg effect: the metabolic requirements of cell proliferation, Science 324 (5930) (2009) 1029–1033, doi: 324/5930/1029 [pii];10.1126/science.1160809 [doi]. [PubMed: 19460998]

[12]. DeBerardinis RJ, Chandel NS, We need to talk about the Warburg effect, Nat. Metab 2 (2) (2020) 127–129, 10.1038/s42255-020-0172-2. [PubMed: 32694689]

[13]. Liemburg-Apers DC, Schirris TJ, Russel FG, Willems PH, Koopman WJ, Mitoenergetic dysfunction triggers a rapid compensatory increase in steady-state glucose flux, Biophys. J 109 (7) (2015) 1372–1386, doi: S0006-3495(15)00784-5 [pii];10.1016/j.bpj.2015.08.002 [doi]. [PubMed: 26445438]

[14]. Robinson GL, Dinsdale D, Macfarlane M, Cain K, Switching from aerobic glycolysis to oxidative phosphorylation modulates the sensitivity of mantle cell lymphoma cells to TRAIL,

Oncogene 31 (48) (2012) 4996–5006. Epub 2012/02/09. doi: 10.1038/onc.2012.13. [PubMed: 22310286]

[15]. Smolkova K, Bellance N, Scandurra F, Genot E, Gnaiger E, Plecita-Hlavata L, Jezek P, Rossignol R, Mitochondrial bioenergetic adaptations of breast cancer cells to aglycemia and hypoxia, J. Bioenergy Biomembr 42 (1) (2010) 55–67, 10.1007/s10863-009-9267-x.

[16]. Fang D, Maldonado EN, VDAC regulation: a mitochondrial target to stop cell proliferation, Adv. Cancer Res 138 (2018) 41–69, 10.1016/bs.acr.2018.02.002. [PubMed: 29551129]

[17]. Maldonado EN, VDAC-tubulin, an anti-warburg pro-oxidant switch, Front. Oncol 7 (2017) 4, 10.3389/fonc.2017.00004. [PubMed: 28168164]

[18]. De PV, Guarino F, Guarnera A, Messina A, Reina S, Tomasello FM, Palermo V, Mazzoni C, Characterization of human VDAC isoforms: a peculiar function for VDAC3? Biochim. Biophys. Acta 1797 (6–7) (2010) 1268–1275, doi: S0005-2728(10)00042-3 [pii];10.1016/j.bbabio.2010.01.031 [doi]. [PubMed: 20138821]

[19]. Sampson MJ, Lovell RS, Craigen WJ, The murine voltage-dependent anion channel gene family. Conserved structure and function, J. Biol. Chem 272 (30) (1997) 18966–18973. [PubMed: 9228078]

[20]. Hiller S, Abramson J, Mannella C, Wagner G, Zeth K, The 3D structures of VDAC represent a native conformation, Trends Biochem. Sci 35 (9) (2010) 514–521, doi: S0968-0004(10)00049-6 [pii];10.1016/j.tibs.2010.03.005 [doi]. [PubMed: 20708406]

[21]. Ujwal R, Cascio D, Colletier JP, Faham S, Zhang J, Toro L, Ping P, Abramson J, The crystal structure of mouse VDAC1 at 2.3 A resolution reveals mechanistic insights into metabolite gating, Proc. Natl. Acad. Sci. USA 105 (46) (2008) 17742–17747, doi: 0809634105 [pii];10.1073/pnas.0809634105 [doi]. [PubMed: 18988731]

[22]. Bowen KA, Tam K, Colombini M, Evidence for titratable gating charges controlling the voltage dependence of the outer mitochondrial membrane channel, VDAC, J. Membr. Biol 86 (1) (1985) 51–59, 10.1007/BF01871610. [PubMed: 2413210]

[23]. Colombini M, Voltage gating in the mitochondrial channel, VDAC, J. Membr. Biol 111 (2) (1989) 103–111. [PubMed: 2482359]

[24]. Colombini M, Structure and mode of action of a voltage dependent anion-selective channel (VDAC) located in the outer mitochondrial membrane, Ann. N. Y. Acad. Sci 341 (1980) 552–563. [PubMed: 6249159]

[25]. Colombini M, VDAC: the channel at the interface between mitochondria and the cytosol, Mol. Cell Biochem 256–257 (1–2) (2004) 107–115.

[26]. Choudhary OP, Ujwal R, Kowallis W, Coalson R, Abramson J, Grabe M, The electrostatics of VDAC: implications for selectivity and gating, J. Mol. Biol 396 (3) (2010) 580–592, doi: S0022-2836(09)01476-4 [pii];10.1016/j.jmb.2009.12.006 [doi]. [PubMed: 20005234]

[27]. Colombini M, The VDAC channel: molecular basis for selectivity, Biochim. Biophys. Acta 1863 (10) (2016) 2498–2502, 10.1016/j.bbamcr.2016.01.019. [PubMed: 26826035]

[28]. Villinger S, Giller K, Bayrhuber M, Lange A, Griesinger C, Becker S, Zweckstetter M, Nucleotide interactions of the human voltage-dependent anion channel, J. Biol. Chem 289 (19) (2014) 13397–13406, 10.1074/jbc.M113.524173. [PubMed: 24668813]

[29]. Colombini M, VDAC structure, selectivity, and dynamics, Biochim. Biophys. Acta 1818 (6) (2012) 1457–1465, 10.1016/j.bbamem.2011.12.026. [PubMed: 22240010]

[30]. Tan W, Colombini M, VDAC closure increases calcium ion flux, Biochim. Biophys. Acta 1768 (10) (2007) 2510–2515, doi: S0005-2736(07)00213-1 [pii];10.1016/j.bbamem.2007.06.002 [doi]. [PubMed: 17617374]

[31]. Sander P, Gudermann T, Schredelseker J, A calcium guard in the outer membrane: Is VDAC a regulated gatekeeper of mitochondrial calcium uptake? Int. J. Mol. Sci 22 (2) (2021) 10.3390/ijms22020946.

[32]. Maldonado EN, Sheldon KL, DeHart DN, Patnaik J, Manevich Y, Townsend DM, Bezrukov SM, Rostovtseva TK, Lemasters JJ, Voltage-dependent anion channels modulate mitochondrial metabolism in cancer cells: regulation by free tubulin and erastin, J. Biol. Chem 288 (17) (2013) 11920–11929, doi: M112.433847 [pii];10.1074/jbc.M112.433847 [doi]. [PubMed: 23471966]

[33]. Rostovtseva TK, Sheldon KL, Hassanzadeh E, Monge C, Saks V, Bezrukov SM, Sackett DL, Tubulin binding blocks mitochondrial voltage-dependent anion channel and regulates respiration, Proc. Natl. Acad. Sci. USA 105 (48) (2008) 18746–18751, doi: 0806303105 [pii];10.1073/pnas.0806303105 [doi]. [PubMed: 19033201]

[34]. Timohhina N, Guzun R, Tepp K, Monge C, Varikmaa M, Vija H, Sikk P, Kaambre T, Sackett D, Saks V, Direct measurement of energy fluxes from mitochondria into cytoplasm in permeabilized cardiac cells in situ: some evidence for Mitochondrial Interactosome, J. Bioenergy Biomembr 41 (3) (2009) 259–275, 10.1007/s10863-009-9224-8.

[35]. Baines CP, Kaiser RA, Sheiko T, Craigen WJ, Molkentin JD, Voltage-dependent anion channels are dispensable for mitochondrial-dependent cell death, Nat. Cell Biol 9 (5) (2007) 550–555. [PubMed: 17417626]

[36]. Das S, Wong R, Rajapakse N, Murphy E, Steenbergen C, Glycogen synthase kinase 3 inhibition slows mitochondrial adenine nucleotide transport and regulates voltage-dependent anion channel phosphorylation, Circ. Res 103 (9) (2008) 983–991, doi: CIRCRESAHA.108.178970 [pii];10.1161/CIRCRESAHA.108.178970 [doi]. [PubMed: 18802025]

[37]. Vander Heiden MG, Li XX, Gotdeib E, Hill RB, Thompson CB, Colombini M, Bcl-xL promotes the open configuration of the voltage-dependent anion channel and metabolite passage through the outer mitochondrial membrane, J. Biol. Chem 276 (22) (2001) 19414–19419. [PubMed: 11259441]

[38]. Bohm R, Amodeo GF, Murlidaran S, Chavali S, Wagner G, Winterhalter M, Brannigan G, Hiller S, The structural basis for low conductance in the membrane protein VDAC upon beta-NADH binding and voltage gating, Structure 28 (2) (2020) 206–14 e4, 10.1016/j.str.2019.11.015. [PubMed: 31862297]

[39]. Christie CF, Fang D, Hunt EG, Morris ME, Rovini A, Heslop KA, Beeson GC, Beeson CC, Maldonado EN, Statin-dependent modulation of mitochondrial metabolism in cancer cells is independent of cholesterol content, FASEB J. (2019), 10.1096/fj.201802723R.

[40]. Maldonado EN, DeHart DN, Patnaik J, Klatt SC, Beck GM, Lemasters JJ, ATP/ADP turnover and import of glycolytic ATP into mitochondria in cancer cells is independent of the adenine nucleotide translocator, J. Biol. Chem (2016) doi: M116.734814 [pii];10.1074/jbc.M116.734814 [doi].

[41]. Rovini A, Heslop K, Hunt EG, Morris ME, Fang D, Gooz M, Gerencser AA, Maldonado EN, Quantitative analysis of mitochondrial membrane potential heterogeneity in unsynchronized and synchronized cancer cells, FASEB J. 35 (1) (2021), e21148, 10.1096/fj.202001693R. [PubMed: 33196122]

[42]. Beeson CC, Beeson GC, Schnellmann RG, A high-throughput respirometric assay for mitochondrial biogenesis and toxicity, Anal. Biochem 404 (1) (2010) 75–81, 10.1016/j.ab.2010.04.040. [PubMed: 20465991]

[43]. Gerencser AA, Neilson A, Choi SW, Edman U, Yadava N, Oh RJ, Ferrick DA, Nicholls DG, Brand MD, Quantitative microplate-based respirometry with correction for oxygen diffusion, Anal. Chem 81 (16) (2009) 6868–6878, 10.1021/ac900881z. [PubMed: 19555051]

[44]. Shi Y, Jiang C, Chen Q, Tang H, One-step on-column affinity refolding purification and functional analysis of recombinant human VDAC1, Biochem Biophys. Res Commun 303 (2) (2003) 475–482, 10.1016/s0006-291x(03)00359-0. [PubMed: 12659842]

[45]. Liu D, Angelova A, Liu J, Garamus VM, Angelov B, Zhang X, Li Y, Feger G, Li N, Zou A, Self-assembly of mitochondria-specific peptide amphiphiles amplifying lung cancer cell death through targeting the VDAC1-hexokinase-II complex, J. Mater. Chem. B 7 (30) (2019) 4706–4716, 10.1039/c9tb00629j. [PubMed: 31364685]

[46]. Zhang F, Angelova A, Garamus VM, Angelov B, Tu S, Kong L, Zhang X, Li N, Zou A, Mitochondrial voltage-dependent anion channel 1-hexokinase-II complextargeted strategy for melanoma inhibition using designed multiblock peptide amphiphiles, ACS Appl. Mater. Interfaces 13 (30) (2021) 35281–35293, 10.1021/acsami.1c04385. [PubMed: 34309373]

[47]. Zhang X, Angelova A, Sun W, Zhang F, Li N, Zou A, A lipidated peptide with mitochondrial membrane localization in human A549 lung cells: from enhanced cell-penetrating properties to biological activity mechanism, ACS Appl. Bio Mater 4 (12) (2021) 8277–8290, 10.1021/acsabm.1c00815.

[48]. Heslop KA, Milesi V, Maldonado EN, VDAC modulation of cancer metabolism: advances and therapeutic challenges, Front. Physiol 12 (2021), 742839, 10.3389/fphys.2021.742839. [PubMed: 34658929]

[49]. DeHart DN, Lemasters JJ, Maldonado EN, Erastin-Like anti-Warburg agents prevent mitochondrial depolarization induced by free tubulin and decrease lactate formation in cancer cells, SLAS Discov. 23 (1) (2018) 23–33, 10.1177/2472555217731556. [PubMed: 29024608]

[50]. DeHart DN, Fang D, Heslop K, Li L, Lemasters JJ, Maldonado EN, Opening of voltage dependent anion channels promotes reactive oxygen species generation, mitochondrial dysfunction and cell death in cancer cells, Biochem. Pharmacol 148 (2018) 155–162, 10.1016/j.bcp.2017.12.022. [PubMed: 29289511]

[51]. Baffy G, Mitochondrial uncoupling in cancer cells: liabilities and opportunities, Biochim. Biophys. Acta Bioenergy 1858 (8) (2017) 655–664, 10.1016/j.bbabio.2017.01.005.

[52]. Nicholls DG, Mitochondrial proton leaks and uncoupling proteins, Biochim. Biophys. Acta Bioenergy 1862 (7) (2021), 148428, 10.1016/j.bbabio.2021.148428.

[53]. Alavian KN, Beutner G, Lazrove E, Sacchetti S, Park HA, Licznerski P, Li H, Nabili P, Hockensmith K, Graham M, Porter GA Jr., Jonas EA, An uncoupling channel within the c-subunit ring of the F1FO ATP synthase is the mitochondrial permeability transition pore, Proc. Natl. Acad. Sci. USA 111 (29) (2014) 10580–10585, 10.1073/pnas.1401591111. [PubMed: 24979777]

[54]. Alavian KN, Li H, Collis L, Bonanni L, Zeng L, Sacchetti S, Lazrove E, Nabili P, Flaherty B, Graham M, Chen Y, Messerli SM, Mariggio MA, Rahner C, McNay E, Shore GC, Smith PJ, Hardwick JM, Jonas EA, Bcl-xL regulates metabolic efficiency of neurons through interaction with the mitochondrial F1FO ATP synthase, Nat. Cell Biol 13 (10) (2011) 1224–1233, 10.1038/ncb2330. [PubMed: 21926988]

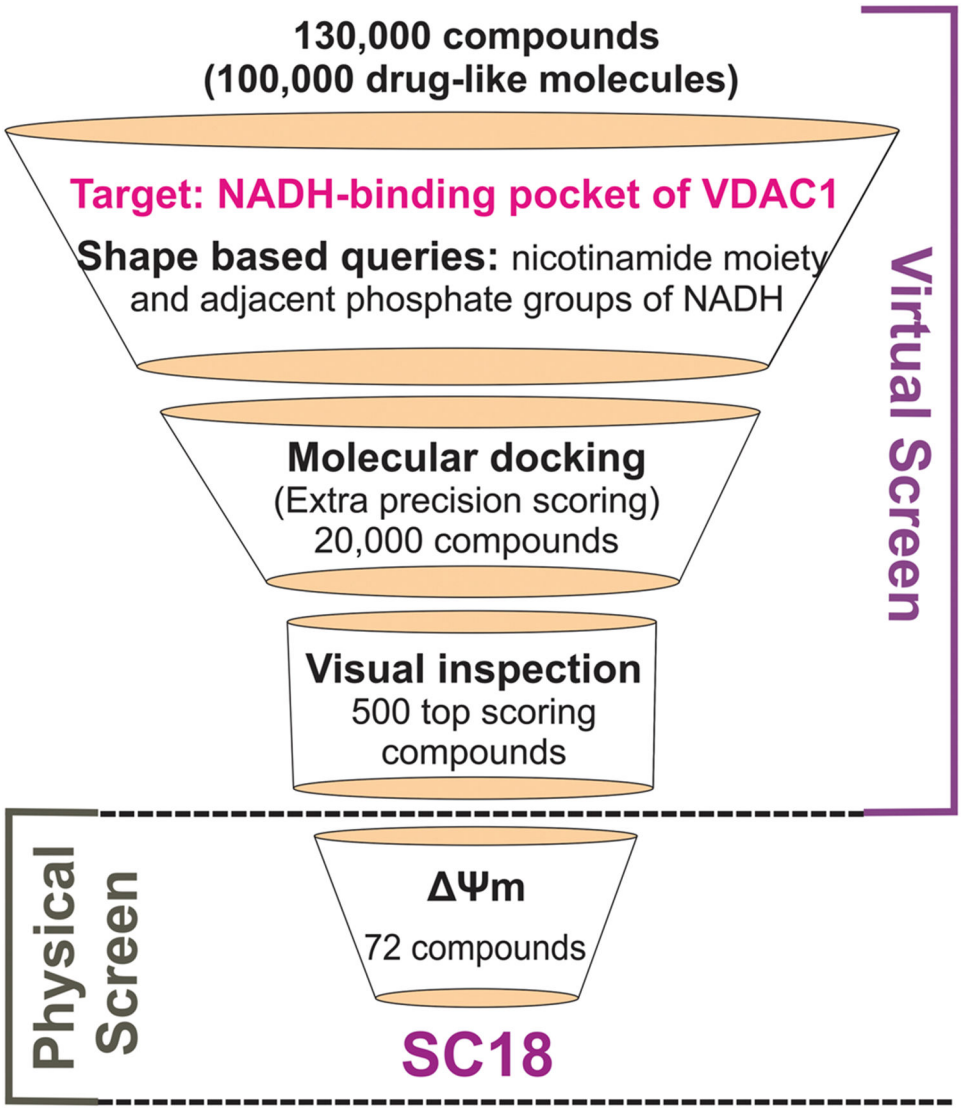

Fig. 1.

Drug screening strategy. *In silico* screening of the South Carolina Compound Collection SC[3] was used for a shape-based query for compounds structurally similar to the nicotinamide moiety and adjacent groups of NADH. The target was the NADH-binding pocket of VDAC1. Selected compounds were subjected to molecular docking and visual inspection of the top scoring compounds. Final 72 compounds were used in a cell-based phenotypic screening, to identify compounds based on the capability of causing a minimum of 40% change in mitochondrial membrane potential. After identification of **SC18**, as the most potent compound, other bioenergetics parameters were evaluated. ΔΨm: mitochondrial membrane potential.

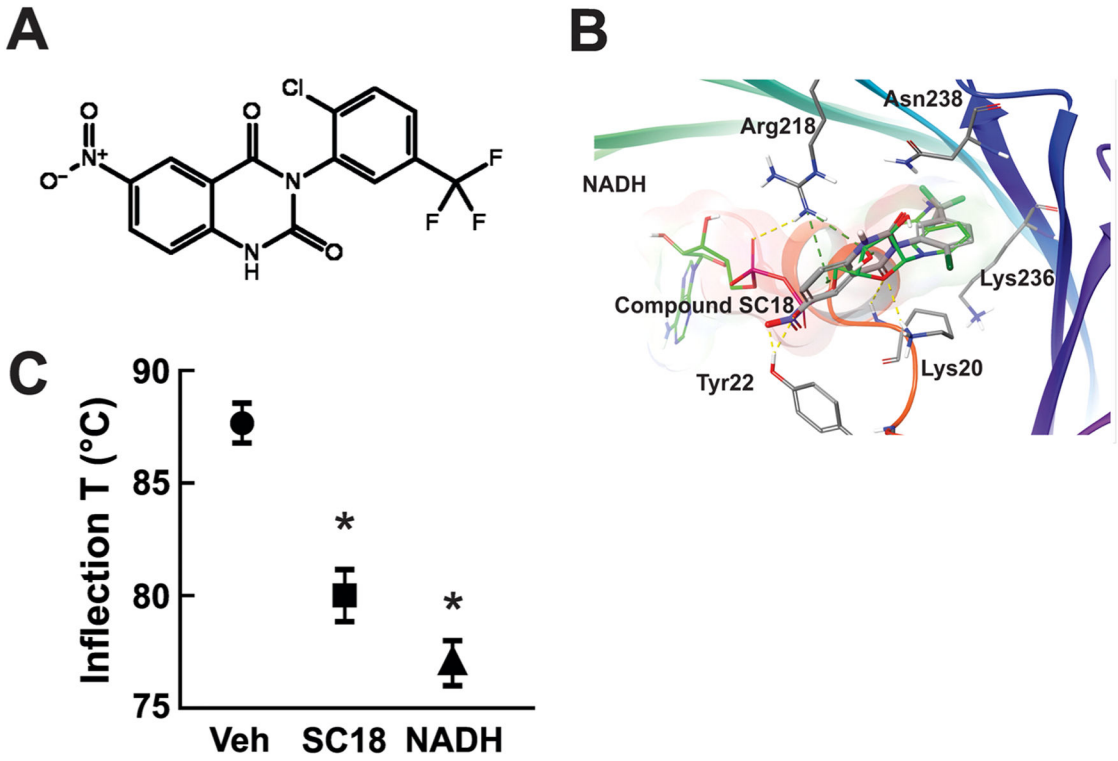

Fig. 2.

SC-18 binds to VDAC. A) Structure of **SC18**. B) Docking of **SC18** to the NADH-binding pocket of VDAC1, revealed pose depicting points of interaction similar to NADH. C) **SC18**, similar to NADH, decreased the inflection temperature at which the protein unfolds, indicating binding of the small molecule to recombinant VDAC1. Arg: Arginine; Asn: asparagine; Lys: lysine; Tyr: tyrosine.

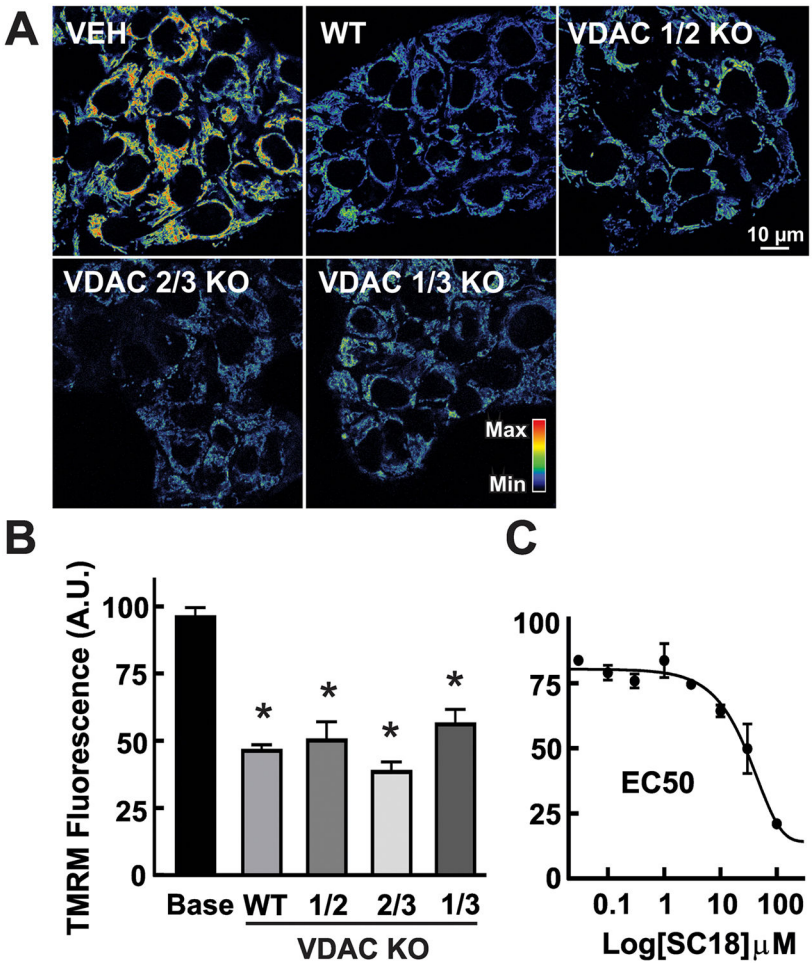

Fig. 3.

SC18 decreases mitochondrial membrane potential. HepG2 cells were loaded with TMRM and treated with **SC18** (25 μM) for 2 h, as described in Materials and Methods. A) **SC18** decreased ΔΨm in WT, VDAC 1/2 KO, 2/3 KO, and 1/3 KO cells. Representative images pseudo-coloured according to the reference bar. B) Quantification of TMRM relative fluorescence after **SC18**. C) The half maximal effective concentration of **SC18** (EC50) was determined using TMRM fluorescence as a readout. * $p < 0.05$ from 3 independent experiments. 4–5 randomly selected fields with 10–20 cells/field were analyzed. a.u.: arbitrary units.

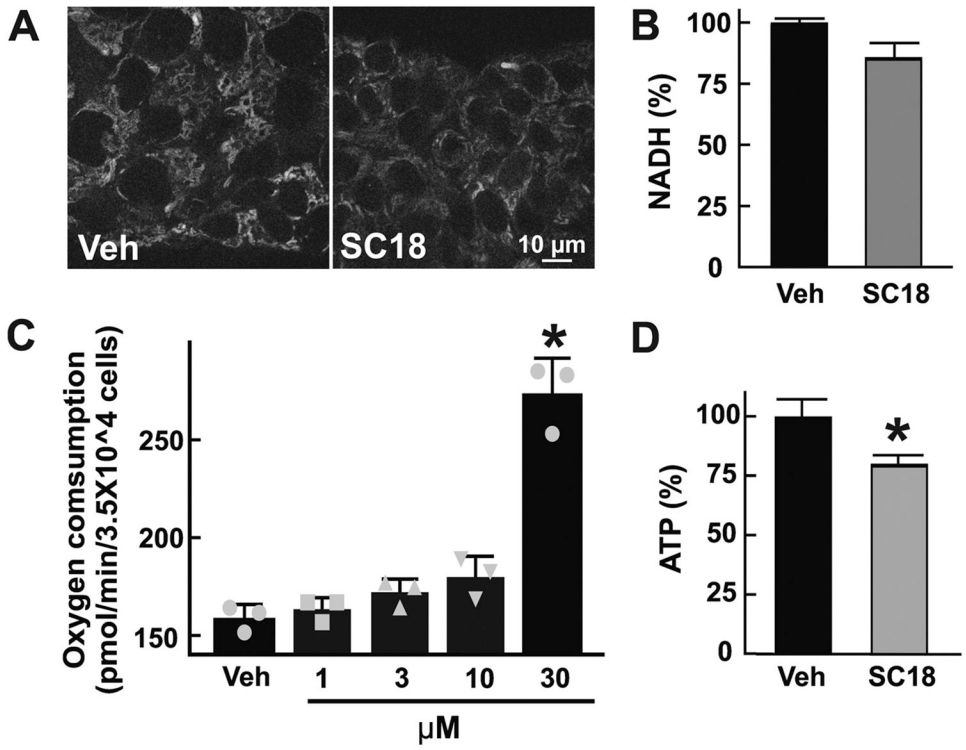

Fig. 4.

Short-term treatment with SC18 modulates cellular bioenergetics. Cells were treated with **SC18** for 2 h. A) **SC18** decreased mitochondrial NADH, assessed by multiphoton confocal microscopy, as described in Materials and Methods. NADH autofluorescence (blue) was converted to gray scale. B) Quantitative analysis of NADH autofluorescence; C) Basal respiration after **SC-18** was determined using a Seahorse XFe96 Analyzer, as described in Material & Methods. D) Cellular ATP was measured using a luciferase based assay. *$p < 0.05$ from 3 independent experiments. 4–5 randomly selected fields with 10–20 cells/field were analyzed for NADH autofluorescence. a.u.: arbitrary units.

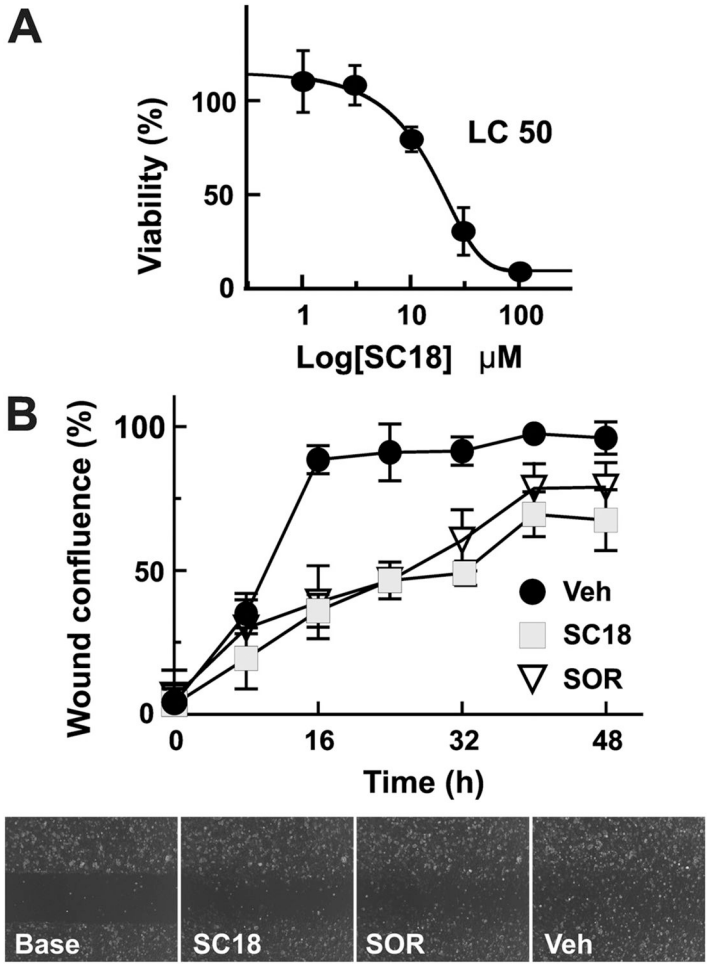

Fig. 5.

SC18 decreased cell proliferation. A) Half the lethal dose of **SC18** (LC50: 23 μM) was calculated from trypan blue exclusion assays. B-C) Wound healing assay: cells were treated with **SC18** (25 μM), sorafenib (5 μM), or vehicle for 48 h. Wound healing was measured at 8 h intervals. Quantitative analysis (upper panel) and representative images (lower panel) *$p < 0.05$ from 3 independent experiments. SOR: sorafenib. Veh: vehicle.